N-terminus oligomerization regulates the function of cardiac ryanodine receptors

Spyros Zissimopoulos[1,*], Cedric Viero[1], Monika Seidel[1], Bevan Cumbes[1], Judith White[1], Iris Cheung[1], Richard Stewart[1], Loice H. Jeyakumar[2], Sidney Fleischer[2], Saptarshi Mukherjee[1], N. Lowri Thomas[1], Alan J. Williams[1] and F. Anthony Lai[1]

[1]Wales Heart Research Institute, Cardiff University School of Medicine, Cardiff CF14 4XN, UK
[2]Departments of Biological Sciences and Pharmacology, Vanderbilt University School of Medicine, Nashville, TN 37232, USA
*Author for correspondence (zissimopouloss@cf.ac.uk)

Accepted 30 July 2013
Journal of Cell Science 126, 5042–5051

doi: 10.1242/jcs.133538

Summary

The ryanodine receptor (RyR) is an ion channel composed of four identical subunits mediating calcium efflux from the endo/sarcoplasmic reticulum of excitable and non-excitable cells. We present several lines of evidence indicating that the RyR2 N-terminus is capable of self-association. A combination of yeast two-hybrid screens, co-immunoprecipitation analysis, chemical crosslinking and gel filtration assays collectively demonstrate that a RyR2 N-terminal fragment possesses the intrinsic ability to oligomerize, enabling apparent tetramer formation. Interestingly, N-terminus tetramerization mediated by endogenous disulfide bond formation occurs in native RyR2, but notably not in RyR1. Disruption of N-terminal inter-subunit interactions within RyR2 results in dysregulation of channel activation at diastolic Ca^{2+} concentrations from ryanodine binding and single channel measurements. Our findings suggest that the N-terminus interactions mediating tetramer assembly are involved in RyR channel closure, identifying a crucial role for this structural association in the dynamic regulation of intracellular Ca^{2+} release.

Key words: Cardiac ryanodine receptor, N-terminus, Calcium release channel, Oligomerization

Introduction

The integral membrane ryanodine receptor (RyR) governs the sarcoplasmic reticulum (SR) Ca^{2+} release that is essential for initiating skeletal muscle contraction and also for triggering the activation of each heartbeat (Zissimopoulos and Lai, 2007). In mammals, RyR1 is the predominant isoform in skeletal muscle, whereas the heart primarily expresses RyR2. The vital importance of RyRs is highlighted in pathological conditions where inherited or acquired defective channel regulation results in abnormal Ca^{2+} handling and leads to neuromuscular disorders, cardiac arrhythmias and heart failure (Blayney and Lai, 2009; George and Lai, 2007). RyRs comprise four identical subunits of ~560 kDa that combine to form high-conductance, cation-permeable channels (Fleischer, 2008). The RyR C-terminus (~10% of the protein) contains the membrane-spanning domains and is known to tetramerize and form a constitutively open Ca^{2+}-conducting pore (Bhat et al., 1997a; Bhat et al., 1997b; George et al., 2004; Wang et al., 1996). The large N-terminal cytoplasmic portion is associated with the transmembrane assembly, as indicated by partial proteolysis studies of native RyR1 (Chen et al., 1993) and by protein complementation assays between overlapping N- and C-terminal RyR2 fragments (George et al., 2004; Masumiya et al., 2003). Intra- and inter-subunit interactions are believed to regulate the opening and closing of the channel pore (Zissimopoulos and Lai, 2007). Importantly, defective inter-domain interactions have been implicated in RyR pathophysiology. For example, Ikemoto, Yano, Matsuzaki and colleagues have proposed that mutation-induced disruption of the association between N-terminal and central domains results in abnormal RyR Ca^{2+} release and is involved in the pathogenesis of malignant hyperthermia (MH) and catecholaminergic polymorphic ventricular tachycardia (CPVT) (Ikemoto and Yamamoto, 2002; Yano et al., 2009).

The N-terminus of RyR1 and RyR2 is the location of one of the three major disease clusters each containing numerous genetic mutations associated with MH and CPVT respectively, implying that it is a functionally important module of the channel. Initial reports using cryo-electron microscopy (EM) of GFP-RyR or GST-RyR protein fusions, or homology modeling and docking analysis, have placed the N-terminus within the clamp region at the corners of the RyR three-dimensional architecture (Baker et al., 2002; Liu et al., 2001; Serysheva et al., 2008; Wang et al., 2007). By contrast, a very different N-terminal topology that specifically located it surrounding the central fourfold axis was recently proposed, based on docking the crystal structure of an RyR1 N-terminal fragment (amino acids 1–559) within the native RyR1 cryo-EM density map (Tung et al., 2010).

Here, we report on the identification of a novel inter-subunit interaction occurring between the N-terminal domains within the RyR2 tetrameric channel and present functional evidence implicating RyR2 N-terminus tetramerization in stabilization of the closed conformation of the channel. Part of these results has previously been presented in abstract form (Zissimopoulos et al., 2005).

Results

RyR2 N-terminus assembles into tetramers

In order to identify whether any of the RyR2 domain(s) associates with the N-terminal fragment of RyR2 (AD4L;

residues 1–906 of human RyR2 fused with GAL4 AD; see Fig. 1), we used the yeast two-hybrid (Y2H) system to screen for the potential protein interaction of AD4L with overlapping RyR2 domain expression constructs spanning the entire protein (Fig. 1). Notably, we found that the human RyR2 N-terminus (AD4L) associated most potently with itself (BT4L; residues 1–906 fused with GAL4 DNA-BD), and weakly interacted with the RyR2 C-terminal tail (BT8) (Fig. 1, inset table). Quantitative β-galactosidase assays indicated a very strong interaction for the BT4L–AD4L association (i.e. N-terminus–N-terminus; Fig. 1, inset histogram), whereas the BT8–AD4L (C-terminus–N-terminus) interaction was considerably weaker (<10%). Central domain constructs (BT5, BT6 and their overlapping BT2 fragment) showed negligible binding to AD4L. These data suggest that the N-terminal portion can specifically confer cogent self-association, thus facilitating RyR2 subunit oligomerization.

To extend the Y2H observations, we co-expressed in mammalian HEK293 cells the RyR2 N-terminus (1–906), differentially tagged with either the Myc or HA peptide epitope (BT4L and AD4L, respectively), and we then performed co-immunoprecipitation (co-IP) assays. HA-AD4L from CHAPS-solubilized HEK293 cell lysate was immunoprecipitated with anti-HA antibodies (Ab^{HA}) and the presence of co-precipitated Myc-BT4L was analyzed by immunoblot using antibodies against Myc (Ab^{Myc}). Initial observations revealed the presence of an oligomeric species and so further experiments were specifically carried out in either reducing (10 mM DTT) or oxidizing (1 mM H_2O_2) conditions. Fig. 2 shows that Myc-tagged BT4L (~100 kDa) was recovered only in the Ab^{HA} IP, and not in the control IP lacking antibody. Without DTT (ambient), an additional Ab^{Myc}-immunoreactive high M_r ($\sim 400\times10^3$) band was detected in the Ab^{HA} IP, indicating that a mixed oligomer had formed comprising BT4L and AD4L. This oligomeric species was abolished by DTT addition, suggesting the existence of disulfide bonding between the protomers. However, the oxidizing reagent H_2O_2 did not substantially enhance conversion of the monomeric into the oligomeric form. Possibly, the same cysteines participating in disulfide bond formation in some subunits are S-glutathionylated or S-nitrosylated in other subunits, thus preventing their oxidation to disulfides. Indeed, it has been reported that several RyR1 cysteines, including cysteines within the N-terminus, displayed all three types of modification; oxidation to RyR1 intra- or inter-subunit disulfide bonds, S-glutathionylation and S-nitrosylation (Aracena-Parks et al., 2006). As the BT4L–AD4L domain is ~100 kDa, formation of the ~400 kDa protein strongly suggests that the RyR2 N-terminus may be self-associating into DTT-sensitive tetramers when expressed in mammalian cells.

Notably, BT4L–AD4L self-interaction occurred in the presence of the reducing agent DTT (Fig. 2), indicating that disulfide bonds are dispensable and RyR2 N-terminal self-association is primarily mediated by non-covalent protein-protein interactions. This was further tested with the use of the linear zwitterionic detergent zwittergent 3-14, which was previously shown to cause dissociation of native RyR1, as well as RyR2 C-terminal tetramers into monomers (Lai et al., 1989; Stewart et al., 2003). We found that zwittergent 3-14 prevented the interaction between BT4L and AD4L in co-immunoprecipitation assays, whereas robust BT4L–AD4L self-interaction was retained in the presence of CHAPS (supplementary material Fig. S1), which suggests that zwittergent 3-14 disrupts non-covalent, RyR2 N-terminal inter-subunit interactions. An alternative explanation is that zwittergent 3-14, as relatively powerful detergent, causes protein conformational changes and/or partial unfolding of the RyR2 N-terminus, thereby preventing its self-association.

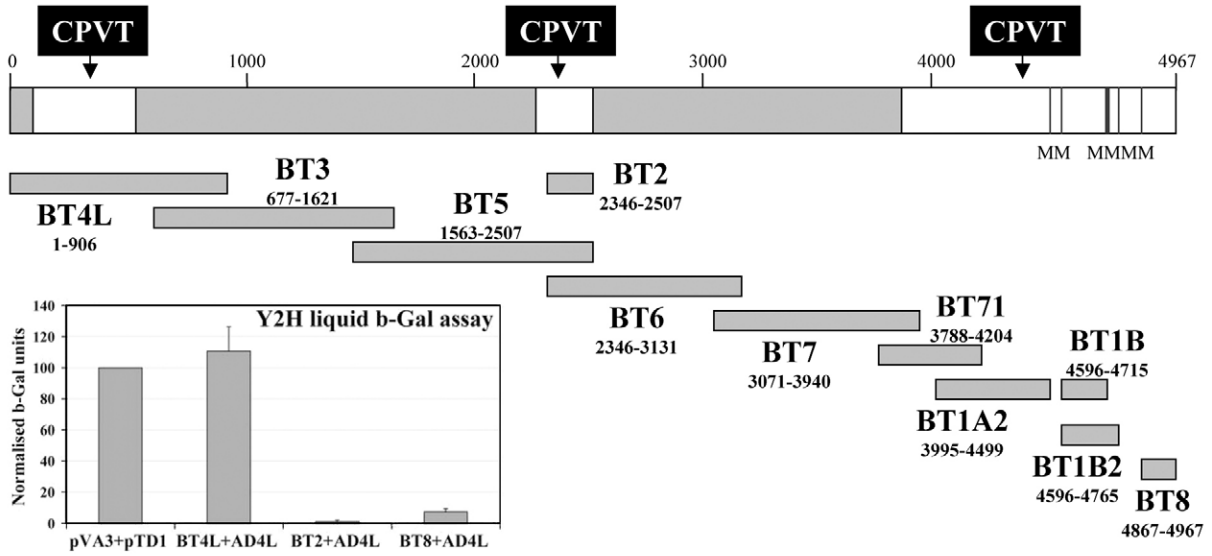

	BT4L (1-906)	BT3 (677-1621)	BT5 (1563-2507)	BT6 (2346-3131)	BT7 (3071-3940)	BT71 (3788-4204)	BT1A2 (3995-4499)	BT1B (4596-4715)	BT1B2 (4596-4765)	BT8 (4867-4967)
AD4L (1-906)	+++++	-	-	-	-	-	-	-	-	+

Fig. 1. The RyR2 N-terminus interacts with itself in yeast cells. Schematic diagram depicting the series of human RyR2 overlapping protein fragments tested in the Y2H system for interaction with the RyR2 N-terminal AD4L construct. Quantitative liquid β-galactosidase assays are shown in the inset (pVA3 encodes GAL4 DNA-BD fusion with p53 protein; pTD1 encodes GAL4 AD fusion with SV40 large T antigen). Results are means ± s.e.m.

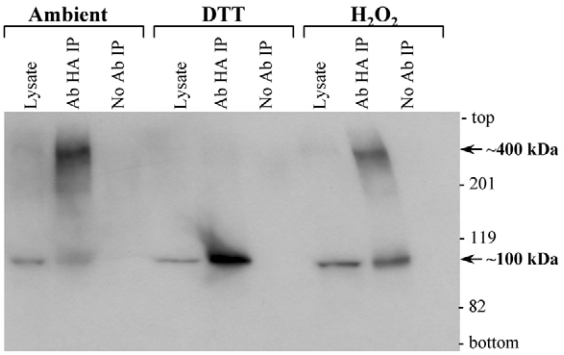

Fig. 2. Self-association of RyR2 N-terminal fragment in mammalian cells. Co-immunoprecipitation assays from HEK293 cell lysate co-expressing Myc-tagged (BT4L) and HA-tagged (AD4L) RyR2 residues 1–906, pre-treated with or without 10 mM DTT or 1 mM H_2O_2 as indicated. AD4L was immunoprecipitated with Ab^{HA} from CHAPS-solubilized HEK293 lysate and the presence of associated BT4L was analyzed by SDS-PAGE (6% gel) and immunoblotting using Ab^{Myc}. Cell lysate, 1/50th of the volume processed in IP samples, was also included to serve as molecular mass standard. Monomer and mixed tetramers are shown with the arrows.

To examine the precise stoichiometry of the RyR2 N-terminus oligomer, we used glutaraldehyde to crosslink HEK293 cell homogenates expressing the ~100 kDa BT4L protein. We observed time-dependent formation of a ~400 kDa band (Fig. 3A,B) indicating existence of a tetrameric assembly of ~100 kDa BT4L protomers, irrespective of DTT pre-treatment. Cumulative data (n=4) following densitometry analysis are presented in Fig. 3C. The predominant protein band observed corresponds to a tetramer, with minimal dimer and no trimer bands detected. Although it is a minor component, the tetrameric form is evident in ambient conditions even before glutaraldehyde addition (i.e. at the 0 minute time point), but is abolished by DTT pre-treatment (0 minute time point, 10 mM DTT) (Fig. 3B). As with the co-IP assays, these experiments indicate that a small proportion of the N-terminus already exists as a disulfide-linked tetramer.

In order to accurately determine the apparent molecular mass of the BT4L oligomer, we used 4–15% gradient SDS-PAGE gels and protein standards with a range of 30–460 kDa (Fig. 3D). From the resulting standard curve, we calculated the oligomer to be 358±15 kDa (n=4), consistent with a tetramer arranged in a closed circular fashion, as expected from the arrangement of the four subunits within the native RyR2 channel. A closed circular tetrameric protein species should experience less gel retardation and would run with greater relative mobility during SDS-PAGE than the equivalent linear form, and therefore it could have an *Rf* that corresponds to a slightly smaller size than the expected 400 kDa. To address whether disulfide bonds are formed by air oxidation during the experiment, we included 5 mM NEM (a thiol-reactive, alkylating reagent) during cell homogenization to covalently modify free sulfhydryls. Tetramers were still obtained after NEM treatment (Fig. 3D), suggesting that sulfhydryl oxidation occurs endogenously within the cells.

During the course of our experiments, the crystal structure of a RyR1 N-terminal fragment (residues 1–559) was determined and topological docking onto the native RyR1 cryo-EM electron density map suggested a tetrameric arrangement (Tung et al., 2010). However, size exclusion chromatography indicated that the purified, bacterially-expressed RyR1 fragment remained a monomer in solution. We therefore used gel filtration to assess oligomerization of the human RyR2(1–906) (GST-BT4L) protein recombinantly expressed in, and purified from, bacteria (supplementary material Fig. S2). Thus, GST-BT4L (~130 kDa) was separated by size exclusion under reducing conditions (10 mM DTT) and then the eluted fractions, analyzed by immunoblot using Ab^{GST}, were compared with gel-filtrated protein standards in the range of 29–669 kDa (Fig. 4). GST-BT4L was detected in two distinct areas of the elution profile, early fractions (46–52 ml) and later elution fractions (64–68 ml) corresponding to the tetramer and monomer, respectively. We note that gel filtration is a technique that separates proteins according to their hydrodynamic size under non-denaturing conditions, and therefore protein oligomers held together by non-covalent protein–protein interactions will be preserved. However, as a result of SDS-PAGE denaturing conditions, which disrupt protein–protein interactions, gel-filtrated GST-BT4L tetramers will dissociate into monomers and a protein band at only ~130 kDa will be detected (Fig. 4A,B). Tetramer formation by purified GST-BT4L was also demonstrated by chemical crosslinking, with no appreciable dimer or trimer bands observed (supplementary material Fig. S3).

Native RyR2 N-terminus assembles into disulfide-linked tetramers

The cumulative evidence from the Y2H, co-IP, chemical crosslinking and gel-filtration data strongly suggest that the discrete RyR2 N-terminus region can tetramerize. However, this oligomerization might not be present in the full-length RyR2, where potentially disparate protein folding of adjacent RyR2 domains and/or accessory regulatory proteins might not favor this interaction. We therefore investigated the oligomeric state of the N-terminus in the native RyR2 from pig cardiac SR, under reducing (10 mM DTT) or oxidizing conditions (1 mM H_2O_2). Native RyR2 was incubated with calpain protease to generate the characteristic ~150 kDa N-terminal and ~400 kDa C-terminal proteolytic fragments. Untreated and calpain-cleaved RyR2 fragments were monitored by immunoblot using two different N-terminal-specific antibodies (Ab^{D2} and Ab^{H300}) and with an antibody against the C-terminus (Ab^{1093}).

On the basis of the results obtained (Fig. 5A,B), we can distinguish between the different possibilities, as follows. Lanes 1, 3 and 5, in the absence of exogenous calpain digestion, show that the full-length RyR2 (550 kDa) subunit is largely intact; however, some degradation by endogenous protease that generates the ~150 kDa N-terminal (and ~400 kDa C-terminal) fragment is also evident. If the RyR2 and its N-terminus exist in monomeric form, only the 550 kDa and ~150 kDa bands should be observed upon immunoblot analysis of the N-terminus. If the RyR2 and its N-terminus exist as tetramers but are not linked by endogenous disulfide bonds, only the 550 kDa and ~150 kDa bands should be observed (tetramers are dissociated as a result of SDS-PAGE denaturing conditions). This is what we observed in Fig. 5A,B lane 3, where samples were treated with the reducing agent, DTT. If the RyR2 and its N-terminus form into tetramers that are covalently linked by endogenous disulfide bonds, then two bands in addition to 550 kDa and ~150 kDa would be expected; the two additional bands would be the full-length tetramer at 2200 kDa and the N-terminus tetramer at ~600 kDa. We

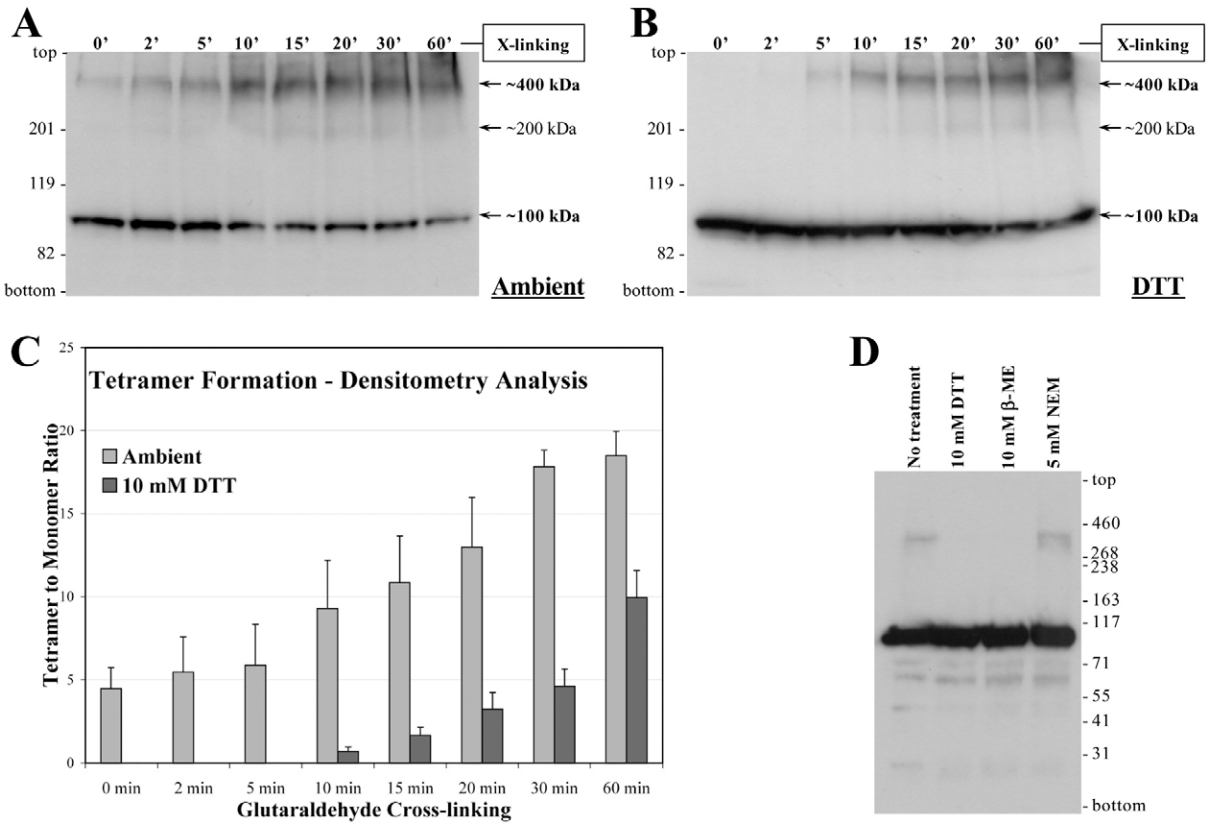

Fig. 3. Tetramer is the predominant oligomeric form of RyR2 N-terminal fragment. (A,B) Chemical crosslinking assays from HEK293 cell homogenate expressing BT4L, pre-treated without (A) or with (B) the reducing agent, dithiothreitol (10 mM DTT). Cell homogenate was incubated with glutaraldehyde for the indicated time points and analyzed by SDS-PAGE (6% gels) and immunoblotting using Ab^{Myc}. Oligomeric forms are indicated by the arrows. (C) Densitometry analysis (n=4) was carried out on the bands corresponding to tetramer and monomer and used to express tetramer to monomer ratio. Data are given as mean value ± s.e.m. (D) HEK293 cells expressing BT4L were homogenized in the presence of 10 mM DTT, 10 mM β-mercaptoethanol or 5 mM N-ethylmaleimide. Proteins were separated through 4–15% gradient SDS-PAGE gel together with high molecular mass markers (HiMark, Invitrogen). A calibration standard curve was subsequently prepared by plotting Rf values versus log M_r and fitting the data using a polynomial curve (not shown).

observed the ~600 kDa, but not the 2200 kDa band in Fig. 5A,B lanes 1 and 5 (ambient and H_2O_2, respectively). The reason why the 2200 kDa band is not visible is most probably due to low abundance and/or poor electrophoretic transfer of such a large protein. Fig. 5A,B lanes 2, 4 and 6, following exogenous calpain digestion, show that the full-length 550 kDa subunit is abolished to yield the ~150 kDa N-terminal fragment (and ~400 kDa C-terminus). If the RyR2 and its N-terminus were monomeric, only the ~150 kDa band should be observed. If the RyR2 and its N-terminus form tetramers that are not linked by endogenous disulfide bonds, only the ~150 kDa band should be observed. This is what we observed in Fig. 5A,B lane 4, where samples were treated with the reducing agent, DTT. If the RyR2 and its N-terminus exist as tetramers that are covalently linked by endogenous disulfide bonds, the N-terminus tetramer at ~600 kDa in addition to the ~150 kDa monomer band would be expected. This is what we observed in Fig. 5A,B lanes 2 and 6 (ambient and H_2O_2, respectively).

Thus, two different antibodies, Ab^{D2} and Ab^{H300}, which recognize different epitopes within the N-terminus, detected a ~600 kDa oligomeric protein (Fig. 5A,B). The band at ~600 kDa persisted following calpain cleavage, but it was abolished by DTT, consistent with disulfide-linked tetramerization of the ~150 kDa N-terminal fragment. Addition of H_2O_2 did not substantially enhance the ~600 kDa species. Densitometry analysis indicated that following exogenous calpain cleavage, the disulfide-linked N-terminus tetramer to monomer relative abundance is 10.8±4.0% and 13.0±4.7% for ambient and H_2O_2 conditions, respectively (n=4). By contrast, Ab^{1093} (specific for RyR2 C-terminus) failed to detect the ~600 kDa band, confirming that it does not contain the RyR2 C-terminus (Fig. 5C). Instead, Ab^{1093} detected a band at ~1600 kDa, which resisted calpain cleavage but was abolished by DTT, which would be consistent with disulfide-linked tetramerization of the ~400 kDa C-terminal fragment. These results suggest that the native pig RyR2 N-terminus region associates with itself and, after calpain cleavage, remains tetrameric through DTT-sensitive disulfide bonds. Note that both the ~600 kDa N-terminus and ~1600 kDa C-terminus tetramers did not appear to substantially increase following exogenous calpain digestion. Interestingly, it seems that native RyR2 subunits that are disulfide-linked are already cleaved by endogenous calpain. This could imply that endogenous calpain digestion primes RyR2 for inter-subunit disulfide linkage. Alternatively, disulfide-linked RyR2 might be specifically targeted for calpain digestion.

Similar calpain cleavage experiments were carried out for native RyR1 from rabbit skeletal muscle SR, using antibodies specific for the N- and C-terminal RyR1 fragments (Ab^{2142} or

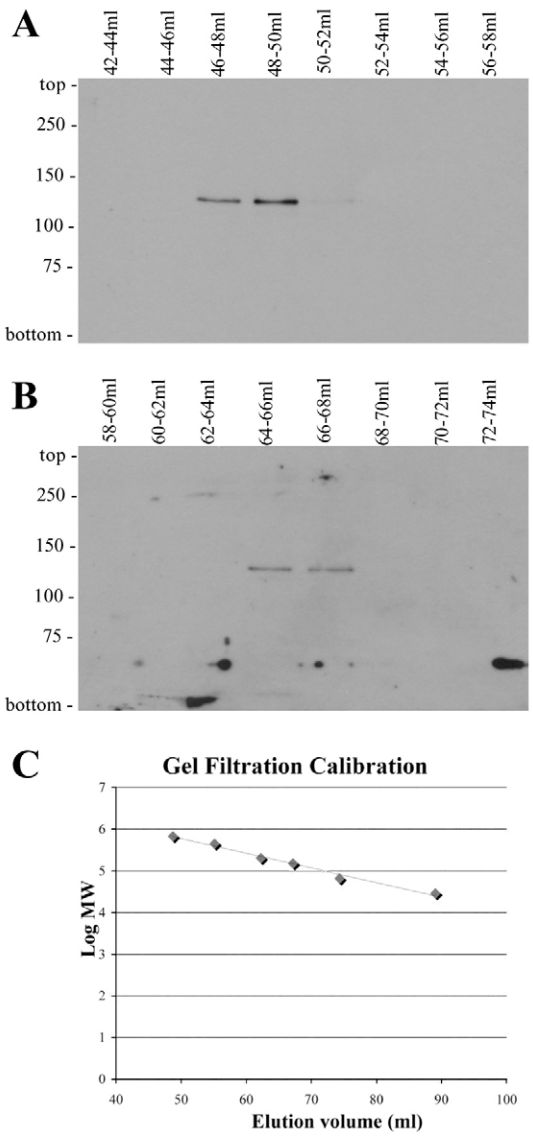

Fig. 4. Gel filtration of purified RyR2 N-terminal fragment. (A,B) Western blot analysis using Ab^{GST} of eluted fractions following gel filtration of purified GST-BT4L (RyR2 residues 1–906). (C) Gel-filtration calibration curve (elution volumes in ml plotted against log M_r) was generated using thyroglobulin (669 kDa), apoferritin (443 kDa), β-amylase (200 kDa), alcohol dehydrogenase (150 kDa), BSA (66 kDa) and carbonic anhydrase (29 kDa).

Ab^{H300} and Ab^{2149}, respectively). Unlike RyR2, the RyR1 ~150 kDa N-terminal fragment was detected only as a monomer, irrespective of the presence of DTT or H_2O_2 (Fig. 5D,E). The RyR1 ~400 kDa C-terminal fragment was found as a monomer (ambient, DTT-treated), but H_2O_2 induced appearance of a ~1600 kDa band, which is consistent with a tetramer (Fig. 5F).

RyR2 N-terminus dissociation enhances channel activity

N-terminus tetramerization confers a structural role, but could also potentially contribute to functional regulation of the RyR2 channel. To assess its putative functional significance, we investigated the effects that the BT4L fragment exerts on the activity of native and recombinant RyR2 channels. Our reasoning was that the exogenous BT4L fragment could compete for N-terminal binding sites presumed to exist within the RyR2 oligomer, thereby disrupting endogenous N-terminal inter-subunit interactions and altering channel function. DTT was included in the assays to reduce the covalent disulfide bonds, leaving only the non-covalent protein–protein interactions within the RyR2 N-terminus, thus facilitating the interaction of exogenous BT4L with the endogenous N-terminal region within the native RyR2 channel. Using GST pull-down assays, we observed that the purified GST-BT4L polypeptide interacts with native RyR2 and the 150 kDa calpain-cleaved N-terminal fragment (supplementary material Fig. S4). Initial [^{3}H]ryanodine binding assays of pig cardiac SR indicated that 10 nM GST-BT4L caused a ~twofold binding increase at low Ca^{2+} concentrations (supplementary material Table S1), although the results did not reach statistical significance. This could be due to the low concentration of GST-BT4L used (dictated by the low protein expression and purification yield from bacteria) and/or insufficient binding assay incubation time.

To overcome this problem of the low yield of isolated protein, we co-expressed BT4L with full-length RyR2 in HEK293 cells, enabling an enhanced concentration of BT4L protein to potentially interact with and disrupt the N-terminus self-association within RyR2 channels upon recombinant expression. Sub-cellular fractionation and immunoblot analysis indicated that the recombinant BT4L specifically translocates from the cytosol to a predominantly microsomal localization only upon co-expression with the full-length RyR2 (supplementary material Fig. S5). [^{3}H]Ryanodine binding assays performed under reducing conditions (2 mM DTT) on HEK293 microsomes that contained either co-expressed RyR2+BT4L, or RyR2 alone, revealed a maximum binding value (in 100 μM free Ca^{2+} and 10 mM caffeine) of 37.9±4.3 and 41.0±3.7 fmol/mg, respectively, indicating equivalent RyR2 protein expression, which was also verified by immunoblotting. The presence of co-expressed BT4L did not affect ryanodine binding to RyR2 at Ca^{2+} ≥1 μM (Fig. 6). By contrast, at low Ca^{2+} concentrations (≤250 nM), the presence of BT4L induced a statistically significant ~twofold increase ($P<0.05$) in ryanodine binding, suggesting that RyR2 channel activation by the recombinant BT4L occurs in low Ca^{2+} conditions.

The functional effects of BT4L on RyR2 activity were further investigated in single-channel recordings. RyR2 from CHAPS-solubilized HEK293 cells isolated by sucrose density gradient centrifugation was incorporated into lipid bilayers and cation channel activity was monitored at 100 nM free cis Ca^{2+}, approximating the diastolic Ca^{2+} concentration in cardiac myocytes. Upon recombinant BT4L polypeptide (+10 mM DTT) addition to the cis chamber, the open probability of a third of RyR2 channels increased, following a variable delay. The unresponsiveness and/or variable delay of some channels could be due to the relatively low (10 nM) BT4L protein concentrations applied, and the kinetic mechanism of BT4L action potentially involving interaction of BT4L with the full-length RyR2 to promote N-terminus dissociation within the oligomeric channel. As shown in Fig. 7A, RyR2 channel activity was extremely low at 100 nM cytosolic Ca^{2+} ($P_o=0.004$). Addition of 10 nM GST-BT4L to the cis chamber resulted in a significant increase of open probability ($P_o=0.064$). Under these conditions, the average increase in P_o by GST-BT4L was 9.8±4.4 fold ($n=5$ channels).

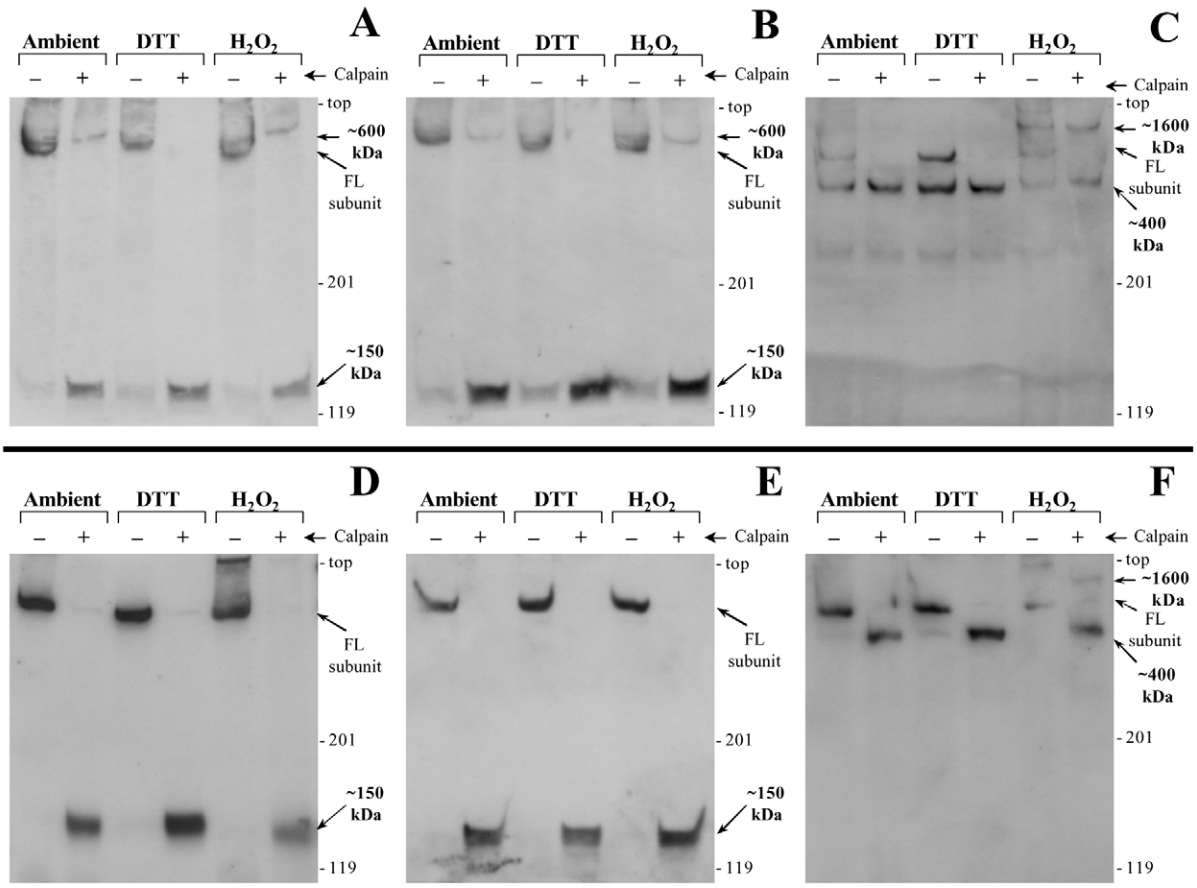

Fig. 5. Native RyR2 N-terminus assembles into disulfide-linked tetramers. Calpain cleavage of pig cardiac SR (A–C) and rabbit skeletal muscle SR (D–F), that were pre-treated with or without 10 mM DTT or 1 mM H_2O_2, as indicated. Samples were analyzed by SDS-PAGE (4% gels) and immunoblotting using Ab^{D2} against RyR2 N-terminus (A), Ab^{H300} against RyR2 N-terminus (B), Ab^{1093} against RyR2 C-terminus (C), Ab^{2142} against RyR1 N-terminus (D), Ab^{H300} against RyR1 N-terminus (E) and Ab^{2149} against RyR1 C-terminus (F). Full-length (FL) RyR subunit, calpain-cleaved ~150 kDa N-terminal and ~400 kDa C-terminal fragments as well as oligomeric forms are indicated by arrows.

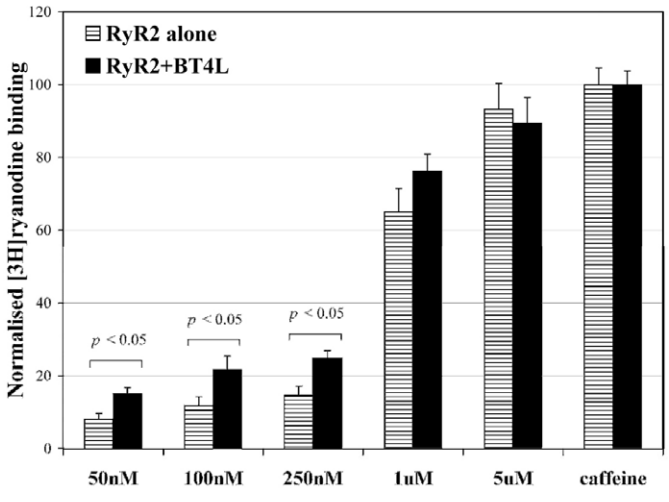

Fig. 6. RyR2 displays increased [^{3}H]ryanodine binding in the presence of BT4L. [^{3}H]ryanodine binding assays of HEK293 microsomes expressing RyR2 alone or RyR2 with BT4L, over a range of free Ca^{2+} concentrations. Summary of three separate experiments each performed at least in duplicate. Data are normalized against maximum binding (obtained in the presence of 100 μM free Ca^{2+} and 10 mM caffeine) and expressed as mean value ± s.e.m.

To control for the GST moiety, we carried out experiments where GST alone and GST-BT4L were sequentially added to the cis chamber. Fig. 7B shows a channel where 100 nM GST alone had a minimal effect (P_o=0.019 for GST versus P_o=0.014 for control), but the subsequent addition of 10 nM GST-BT4L resulted in a substantially increased open probability (P_o=0.084). On average, GST-BT4L increased P_o by 7.4±2.8 fold relative to GST alone (n=5 channels). The two datasets pooled together indicate that GST-BT4L specifically induced a statistically significant (P<0.05) increase in channel P_o by 8.6±2.5 fold (n=10 channels). By contrast, GST alone resulted in a 1.7±0.4-fold increase in P_o (n=7 channels).

Discussion

The aim of our study was to identify the RyR2 domain(s) that potentially interact with the N-terminus to further elucidate its precise structural and functional role. Our Y2H screening of a series of overlapping fragments spanning the entire RyR2 coding sequence revealed that the N-terminus region, BT4L (residues 1–906), interacts strongly with itself (Fig. 1). This self-interaction was verified in HEK293 mammalian cells by co-IP assays using disparate fusion tags (Fig. 2), whereas chemical crosslinking experiments indicated tetramer formation by the N-terminus

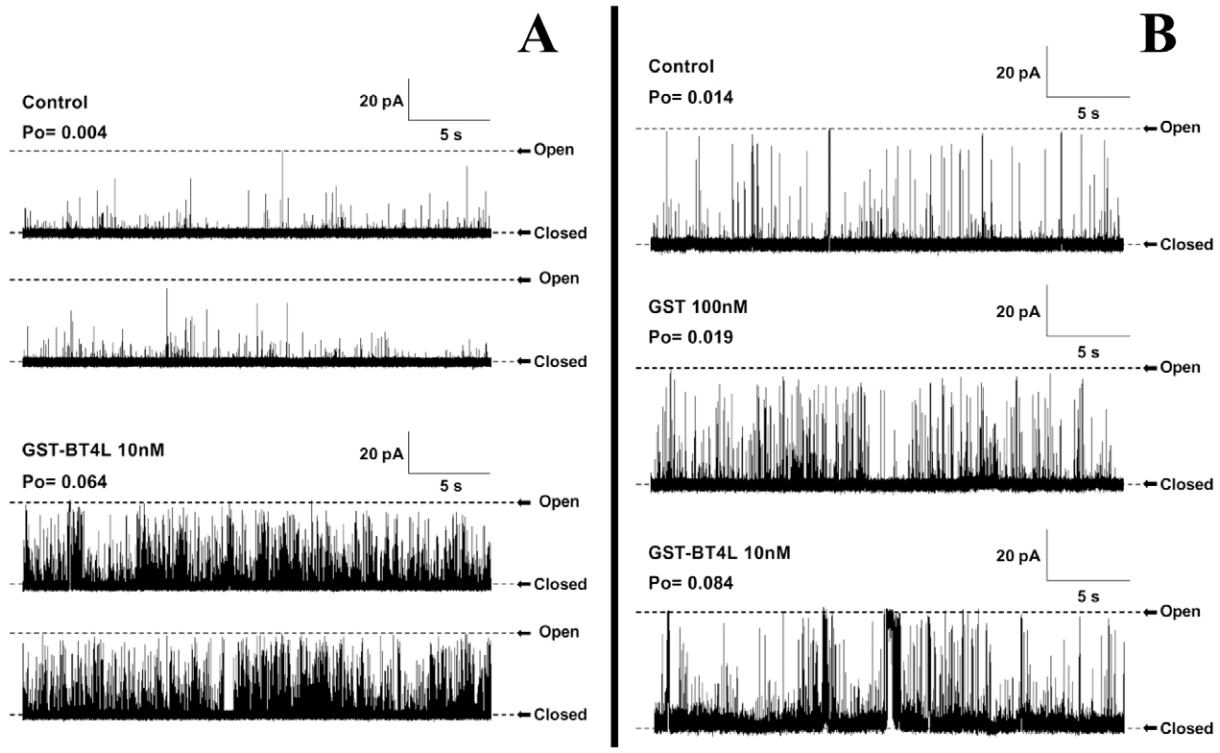

Fig. 7. BT4L enhances RyR2 channel open probability. Single-channel recordings of RyR2 using K^+ as the charge carrier at −60 mV in the presence of cis 100 nM free Ca^{2+}. (A) Channel activity before and after addition of 10 nM GST-BT4L to the cis chamber. (B) Channel activity before and after sequential addition to the same channel of 100 nM GST alone, followed by 10 nM GST-BT4L, in the cis chamber. Please note the difference in scale bars between A and B.

domain (Fig. 3). Consistent with this observation, a tetrameric species was also identified by gel filtration of the purified N-terminal fragment (Fig. 4). Interestingly, in the native pig heart RyR2, the N-terminus was found to form stable tetramers involving intrinsic disulfide bonds (Fig. 5). However, disulfide bonds appear not to be essential for N-terminal oligomerization, because the discrete RyR2 N-terminus domain was still able to form tetramers in the presence of DTT (Fig. 3B; Fig. 4). These findings suggest that the RyR2 N-terminus domain can intrinsically assemble into tetramers through non-covalent protein–protein interactions, and that N-terminal tetramerization could be further stabilized by covalent bonds between cysteine residues in the native protein. The observed tetramerization favors a model where the N-terminal regions of the four subunits within a single RyR2 channel are associated with each other in a closed circular fashion (Fig. 8). If the N-termini were involved in inter-oligomeric interaction between adjacent channels within the two-dimensional membrane lattice (Yin et al., 2005; Yin and Lai, 2000), the formation of dimers rather than tetramers would be expected. This is because tetramer assembly (or any oligomer >2) should in theory be mediated by at least two interacting domains per monomer, whereas a single site of interaction would only lead to dimers.

Our model for RyR2 N-terminus tetramerization based on empirical evidence derived from the current biochemical analysis

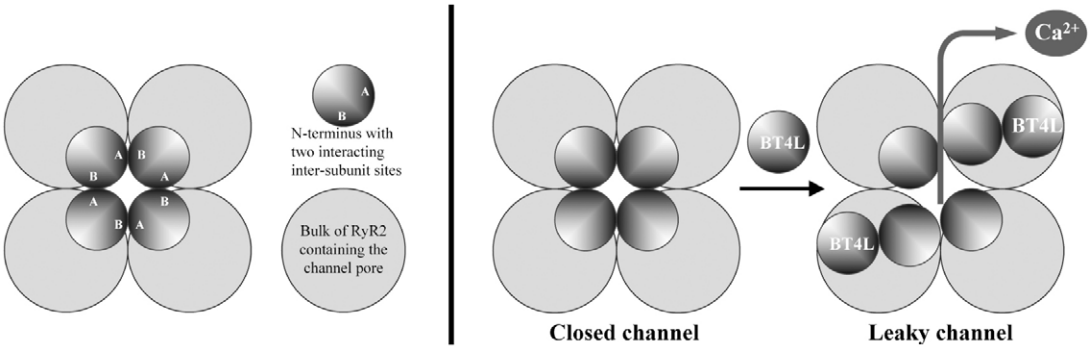

Fig. 8. Proposed model of RyR2 N-terminus tetramerization. Drawing on the left is a schematic representation of the RyR2 N-terminus interactions that form a tetramer surrounding the central fourfold axis. A simplified model of proposed RyR2 N-terminus dissociation induced by exogenous BT4L peptide resulting in a 'leaky' channel is shown on the right.

(Fig. 8), appears incompatible with the proposed 'clamp' location for the N-terminus at the periphery of the RyR initially suggested by cryo-EM studies of GFP-RyR or GST-RyR fusions and/or homology modeling and docking (Baker et al., 2002; Liu et al., 2001; Serysheva et al., 2008; Wang et al., 2007). By contrast, our N-terminal tetramerization model is entirely consistent with, and supports the recently proposed N-terminus location surrounding the central fourfold axis of RyR1 (Tung et al., 2010). Although the N-terminal fragment of RyR1 (amino acids 1–559) remained a monomer in the crystal, a precise docking of its tertiary structure within the native RyR1 EM density map placed the four N-terminal domains immediately adjacent to each other at the center of the molecule (Tung et al., 2010). In the previous studies, GST or GFP was fused at the extreme N-terminus of RyR3 or at Ser437 within RyR2, respectively, and observed differences in the resultant cryo-EM density maps relative to wild-type RyR2 or RyR3, were taken as evidence for the precise location of the GST or GFP insertion (Liu et al., 2001; Wang et al., 2007). However the insertion of GST or GFP, both discrete proteins of ~27 kDa, potentially could have perturbed the intrinsic RyR structure locally and might also induce long-range allosteric effects. Hence, distally-altered RyR conformational changes (e.g. at the RyR periphery) might result from N-terminal GST or GFP insertions (e.g. at the RyR centre) and are therefore attributed incorrectly as the actual location of the N-terminus. Additionally, cryo-EM sample processing involving freezing of solubilized RyR might potentially cause conformational changes in GST-RyR and GFP-RyR fusion proteins that do not occur in the native or wild-type recombinant RyR. Furthermore, the use of long flexible linkers on either side of the insertion, together with the size of a GST or GFP protein, could span a sphere of ~8 nm radius, as already highlighted by Tung and colleagues (Tung et al., 2010).

In other studies, computational methods were used to generate structural models for the RyR1 N-terminus, which were subsequently docked into the clamp region of the full-length RyR1 architecture (Baker et al., 2002; Serysheva et al., 2008). Although the model generated based on the prediction that the RyR1 N-terminus forms an oxidoreductase-like domain (Baker et al., 2002) is not consistent with the structure empirically determined by X-ray crystallography (Tung et al., 2010), the model that was based on the crystal structures of inositol trisphosphate binding core and suppressor domains (Serysheva et al., 2008) is quite similar. However, as previously raised by Tung and colleagues, docking of the latter model at the RyR1 clamps might have been an artifact due to the very electron-dense nature of the clamp region (Tung et al., 2010). Thus, it appears that the initial studies (Baker et al., 2002; Liu et al., 2001; Serysheva et al., 2008; Wang et al., 2007) placing the N-terminus within the clamp region at the corners of the RyR architecture are not compatible with the empirically determined N-terminal location at the centre of the RyR.

Unlike RyR2, we did not detect disulfide-linked N-terminal tetramers for the native RyR1 (Fig. 5D,E) in agreement with a previous report (Wu et al., 1997). However, this does not exclude the presence of RyR1 N-terminal inter-subunit interactions, but simply argues against the requirement for disulfide bonds. Potentially, the RyR2 N-terminal cysteines involved in disulfide bonds are not conserved in RyR1 or else they might be post-translationally modified (e.g. glutathionylation, nitrosylation) in RyR1. Alternatively, these cysteines could be occluded in RyR1 because local conformational differences prevent their oxidation into disulfides. Interestingly, the disparate local folding between skeletal and cardiac RyR N-termini has previously been proposed to explain the differential effects of dantrolene. Despite its binding site being 100% conserved (RyR1 residues 590–609 is identical to RyR2 residues 601–620) and observation of dantrolene binding to RyR1, the wild-type RyR2 does not appear to bind this drug (Paul-Pletzer et al., 2002; Paul-Pletzer et al., 2005). However, dantrolene is capable of inhibiting the failing or mutant (R2474S) RyR2 and can restore normal cardiac function (Kobayashi et al., 2009; Kobayashi et al., 2010; Uchinoumi et al., 2010), suggesting that its interaction site on RyR2 is conformation sensitive, becoming accessible only in disease states. Notably, disulfide-linked N-terminal oligomers were induced in solubilized, purified RyR1 possibly because altered folding exposes previously buried cysteine(s) residues (Wu et al., 1997). Given the high degree of N-terminus sequence homology between the three mammalian RyRs (~85% similarity for residues 1–900 of RyR1, RyR2 and RyR3), the determinants of N-terminus tetramerization could therefore be conserved in all three isoforms. However, although both RyR2 and RyR1 might be capable of N-terminus self-association, cysteine oxidation to form inter-subunit disulfide bonds might occur in an isoform- or tissue-dependent manner.

An intimate association between the RyR N-terminal and central domains has been suggested previously with well-documented functional effects of central-domain-derived, short synthetic peptides (DP4; RyR1 amino acids 2442–2477 and DPc10; RyR2 amino acids 2460–2495) (Ikemoto and Yamamoto, 2002; Yano et al., 2009). However, our Y2H screen notably failed to detect any interaction between the AD4L N-terminal fragment and any of the RyR2 central domain constructs. It is possible that the RyR2 central domain fragments that we used in the present study have an altered, non-native protein conformation that precludes access of the N-terminus to the DPc10 sequence, or prevents the reporter gene transcription necessary for the Y2H protein interaction assay. An alternative explanation is that the robust BT4L self-interaction detracts from the detection of significantly weaker interactions with other RyR2 domains. The use of a series of small N-terminus truncated constructs could possibly help in accurately dissecting the specific sequences involved in mediating N-terminal self-interaction versus central domain binding.

It is apparent that RyR2 N-terminus tetramerization may have more than just a structural role. We observed that RyR2 co-expressed with the N-terminus fragment, BT4L, displayed a ~twofold increase in [^{3}H]ryanodine binding at low Ca^{2+} concentrations (≤250 nM) (Fig. 6 and supplementary material Table S1). At 100 nM Ca^{2+}, exogenous BT4L increased the channel open probability by ~eightfold (Fig. 7). These results indicate that BT4L enhances activity at low Ca^{2+} concentrations, with both native and recombinant purified RyR2 channels, suggesting that its effect on RyR2 is direct, not requiring any other cytosolic proteins. BT4L might be exerting its functional effects by competing with the corresponding RyR2 subunit N-terminal sequence for its local binding partner, thereby disrupting endogenous inter-domain associations of the oligomeric N-terminus in the native RyR2. Further, exogenous BT4L was found to interact with RyR2 and in particular with its N-terminus (supplementary material Fig. 4). Given the wide array of biochemical data consistent with N-terminus self-association, it

seems reasonable to predict that when exogenous BT4L interacts with full-length RyR2, the primary site of its interaction is with the N-terminus of one of the four subunits. In doing so, BT4L displaces the N-terminal domain of this subunit from its tetrameric association with the other three N-termini, thus resulting in disruption or destabilization of the native N-terminal inter-subunit interactions (Fig. 8). We note that rather than being direct evidence, this is the most likely interpretation for the mechanism of action of exogenous BT4L in enhancing RyR2 channel activity.

Thus, stable N-terminus oligomerization is likely to play a functional role in maintaining the RyR2 channel closed at low Ca^{2+}. Accordingly, conditions that weaken or disrupt these oligomeric interactions within the RyR2 N-terminus could lead to SR Ca^{2+} leak during the diastolic phase in cardiac myocytes. RyR2 bearing CPVT mutations are known to result in 'hyper-sensitive' channels and diastolic Ca^{2+} leak, often leading to delayed after-depolarizations and fatal arrhythmias (Blayney and Lai, 2009; Thireau et al., 2011). In light of the present findings, the potential involvement of RyR2 N-terminus tetramerization in the pathogenesis of CPVT is very plausible and this prospect should be further investigated. Indeed, a recent study suggested that the N-terminal region is involved in Ca^{2+} release termination, which could be defective in RyR2-associated cardiomyopathies (Tang et al., 2012).

In summary, we have identified the N-terminus as an important RyR2 structural locus that plays a direct role in promoting channel closure. First, we find that the N-termini of the four RyR2 subunits within a channel assemble into stable tetramers. Second, we present evidence for RyR2-specific, inter-subunit disulfide bonds located specifically within the N-terminal region. Third, disruption of inter-subunit N-terminal interactions enhances channel activity at diastolic Ca^{2+} concentrations consistent with a 'leaky' phenotype. We therefore suggest that defective N-terminal tetramerization has an important role in RyR2 pathophysiology.

Materials and Methods

Materials

Cell culture reagents were obtained from Invitrogen (Life Technologies), high molecular weight markers (HiMark) from Invitrogen (Life Technologies), all other electrophoresis reagents from Bio-Rad, protease inhibitor cocktail (Complete) from Roche, CHAPS and calpain-2 from Calbiochem (Merck), [^{3}H]ryanodine from Perkin-Elmer, synthetic 1-palmitoyl-2-oleoyl-*sn*-glycero-3-phosphoethanolamine from Avanti Polar Lipids; all other reagents from Sigma.

Chemical crosslinking assays

HEK293 cells were homogenized on ice (in 0.3 M sucrose, 5 mM HEPES, pH 7.4 and protease inhibitors) by 20 passages through a needle (23 G, 0.6×25 mm) and dispersing the cell suspension through a half volume of glass beads (425–600 µm). Cell nuclei and glass beads were removed by centrifugation at 1500 ***g*** for 10 minutes at 4℃, and the supernatant was retained. Cell homogenate (20 µg) was incubated with or without 10 mM DTT for 30 minutes and then incubated with 0.0025% glutaraldehyde. Reaction was stopped with 2% hydrazine and SDS-PAGE loading buffer (60 mM Tris-HCl, 2% SDS, 10% glycerol, 5 mM EDTA, 0.01% Bromophenol Blue, pH 6.8) and samples were then analyzed by immunoblotting using Ab^{Myc}.

Calpain cleavage of native RyR1/2

Rabbit skeletal muscle SR (10 µg) or pig cardiac SR (100 µg) was treated with redox reagent (10 mM DTT or 1 mM H_2O_2) for 30 minutes (in 10 mM Na_2PIPES, 120 mM KCl, pH 7.4). SR vesicles were recovered at 20,000 ***g*** for 10 minutes at 4℃, resuspended in fresh buffer supplemented with 2 mM $CaCl_2$ and incubated with 4 units of calpain-2 for 2 minutes at room temperature. Proteolysis was stopped with SDS-PAGE loading buffer and analyzed by immunoblotting using RyR antibodies.

Protein expression and purification, and gel filtration of GST-BT4L

GST-BT4L with C-terminal 6×His tag was created by PCR in pGEX6P1 (GE Healthcare). Protein expression in bacteria (*E.coli* Rosetta, Novagen) was induced for 18 hours at 12℃ with 0.1 mM isopropyl β-D-thiogalactoside at OD_{600}=0.8. Bacteria were permeabilized in PBS (137 mM NaCl, 2.7 mM KCl, 10 mM Na_2HPO_4, 1.8 mM KH_2PO_4, pH 7.4, 10 mM DTT and protease inhibitors) by three freeze-thaw and sonication cycles, and the insoluble material was removed at 10,000 ***g*** for 10 minutes at 4℃. The supernatant was incubated with glutathione-Sepharose (GE Healthcare) for 2 hours at 4℃ and the captured GST-BT4L was eluted with 10 mM glutathione. Eluate was dialyzed (SnakeSkin 10,000 M_r cut-off, Pierce) against buffer (50 mM NaH_2PO_4, 300 mM NaCl, 5 mM β-mercaptoethanol) and incubated with Ni-NTA agarose (Qiagen) for 2 hours at 4℃. Captured GST-BT4L was eluted with 250 mM imidazole and dialyzed against PBS (+10 mM DTT).

A Hiload 16/60 Superdex 200 PG column (GE Healthcare), pre-equilibrated in buffer (10 mM HEPES, 250 mM KCl, 10 mM DTT, pH 7.4), was calibrated with thyroglobulin, apoferritin, β-amylase, alcohol dehydrogenase, BSA and carbonic anhydrase (Sigma) using a 1 ml sample loop on an ÄKTA FPLC (GE Healthcare) at 4℃ with a flow rate of 0.5 ml/minute. GST-BT4L (10 µg), purified in the same buffer, was separated under identical conditions, 2 ml elution fractions were collected and analyzed by immunoblotting using Ab^{GST}.

[^{3}H]Ryanodine binding assays

Ryanodine binding was performed using 8 nM [^{3}H]ryanodine and 200 µg of HEK293 microsomes for 2 hours at 37℃ (in 25 mM PIPES, 1 M KCl, 2 mM DTT, pH 7.4). Free Ca^{2+} concentration was buffered using a combination of $CaCl_2$ and 1 mM EGTA, HEDTA and NTA (calculated using MaxChelator software, www.stanford.edu/~cpatton/downloads.htm). Bound [^{3}H]ryanodine was separated from unbound by vacuum filtration through glass fiber filters (Whatman GF/F). Radioactivity was quantified by liquid scintillation counting. Specific binding was calculated from total by subtracting non-specific binding (in 10 µM unlabelled ryanodine) from three separate experiments, each performed at least in duplicate.

Purification of recombinant RyR2

HEK293 cells transfected with human RyR2 cDNA expression plasmid were homogenized and microsomes pelleted at ~100,000 ***g*** (28,000 rpm, Beckman 50.2Ti rotor) for 1 hour at 4℃. The pellet was solubilised for 1 hour at 4℃ in buffer (25 mM Na_2PIPES, 1 M NaCl, 0.6% CHAPS, 0.6% phosphatidylcholine, 0.15 mM $CaCl_2$, 0.1 mM EGTA, 2 mM DTT, pH 7.4, and protease inhibitors) and the insoluble material was removed at 14,000 ***g*** for 30 minutes at 4℃. The supernatant was layered on top of a continuous (5–40%) sucrose gradient prepared in buffer (25 mM Tris-HCl, 50 mM HEPES, 300 mM NaCl, 0.3% CHAPS, 0.3% phosphatidylcholine, 0.1 mM $CaCl_2$, 0.3 mM EGTA, 2 mM DTT, pH 7.0). The gradient was spun at ~100,000 ***g*** (28,000 rpm, Beckman 32Ti rotor) for 18 hours at 4℃, and fractions were collected. Typically, the ~26–28% sucrose fraction contained functional RyR2 channels.

Single-channel recordings

Planar phospholipid bilayers using phosphatidylethanolamine were formed across a 200-µm-diameter hole in a partition that separated the cis and trans chambers containing 20 mM HEPES, 210 mM KCl, pH 7.2. Purified RyR2 was added to the cis chamber and channel incorporation was induced by the addition of aliquots of 3 M KCl. After fusion, the cis chamber was perfused to re-establish symmetrical 210 mM K^+ and the presence of active single RyR2 channels was verified by recording at −60 mV in contaminating Ca^{2+}. Ca^{2+} dependence was tested by cis addition of 1 mM EGTA, HEDTA and NTA that should cease channel activity; cis free Ca^{2+} concentration was then adjusted to 100 nM. Single-channel current fluctuations were low-pass filtered at 5 kHz, digitized at 20 kHz and displayed with Acquire 5.0.1 software (Bruxton Corporation). To characterize the effect of GST-BT4L (+10 mM DTT) on RyR2, at least 120 seconds of recording data were analyzed for each channel using QuB software (SUNY, Buffalo, www.qub.buffalo.edu). Currents were idealized using the hidden-Markov modeling algorithm of the QuB 1.5.0.39 suite using a simple two state scheme (closed ⇄ open).

Other methods

The yeast two-hybrid system, HEK293 cell culture and transfection, SR preparation, co-immunoprecipitation, GST pull-down assays and immunoblotting were carried out as described previously (Zissimopoulos and Lai, 2005; Zissimopoulos et al., 2006). RyR1-specific Ab^{2142} was raised against residues 830–845, RyR consensus Ab^{2149} was raised against residues 4933–4948 of RyR2, RyR2-specific Ab^{1093} was raised against residues 4454–4474 (Fitzsimmons et al., 2000; Mackrill et al., 1997; Zissimopoulos et al., 2007); RyR2-specific Ab^{D2} (raised against residues 1344–1365) has been described previously (Jeyakumar et al., 2001); RyR consensus Ab^{H300} (raised against N-terminal 300 residues) was obtained from Santa Cruz Biotechnology. Densitometry analysis was performed using a GS-700 scanner (Bio-Rad) and Quantity One software (Bio-Rad).

Statistical analysis was performed using unpaired Student's *t*-test. Data are expressed as mean values ± s.e.m.

Author contributions

S.Z. conceived the study, designed the experiments and wrote the paper; F.A.L. and A.J.W. contributed to study design; S.Z., C.V., M.S., B.C., J.W., I.C., R.S., S.M., N.L.T. performed and analyzed the experimental data; L.H.C. and S.F. contributed reagents and materials; S.Z. and F.A.L. edited the manuscript.

Funding

This work was supported by a British Heart Foundation Fellowship [grant number FS/08/063 to S.Z.]; and Wales Heart Research Institute Training Placement Scholarships to J.W. and I.C.

Supplementary material available online at
http://jcs.biologists.org/lookup/suppl/doi:10.1242/jcs.133538/-/DC1

References

Aracena-Parks, P., Goonasekera, S. A., Gilman, C. P., Dirksen, R. T., Hidalgo, C. and Hamilton, S. L. (2006). Identification of cysteines involved in S-nitrosylation, S-glutathionylation, and oxidation to disulfides in ryanodine receptor type 1. *J. Biol. Chem.* **281**, 40354-40368.

Baker, M. L., Serysheva, I. I., Sencer, S., Wu, Y., Ludtke, S. J., Jiang, W., Hamilton, S. L. and Chiu, W. (2002). The skeletal muscle Ca^{2+} release channel has an oxidoreductase-like domain. *Proc. Natl. Acad. Sci. USA* **99**, 12155-12160.

Bhat, M. B., Zhao, J., Takeshima, H. and Ma, J. (1997a). Functional calcium release channel formed by the carboxyl-terminal portion of ryanodine receptor. *Biophys. J.* **73**, 1329-1336.

Bhat, M. B., Zhao, J., Zang, W., Balke, C. W., Takeshima, H., Wier, W. G. and Ma, J. (1997b). Caffeine-induced release of intracellular Ca^{2+} from Chinese hamster ovary cells expressing skeletal muscle ryanodine receptor. Effects on full-length and carboxyl-terminal portion of Ca^{2+} release channels. *J. Gen. Physiol.* **110**, 749-762.

Blayney, L. M. and Lai, F. A. (2009). Ryanodine receptor-mediated arrhythmias and sudden cardiac death. *Pharmacol. Ther.* **123**, 151-177.

Chen, S. R., Airey, J. A. and MacLennan, D. H. (1993). Positioning of major tryptic fragments in the Ca^{2+} release channel (ryanodine receptor) resulting from partial digestion of rabbit skeletal muscle sarcoplasmic reticulum. *J. Biol. Chem.* **268**, 22642-22649.

Fitzsimmons, T. J., Gukovsky, I., McRoberts, J. A., Rodriguez, E., Lai, F. A. and Pandol, S. J. (2000). Multiple isoforms of the ryanodine receptor are expressed in rat pancreatic acinar cells. *Biochem. J.* **351**, 265-271.

Fleischer, S. (2008). Personal recollections on the discovery of the ryanodine receptors of muscle. *Biochem. Biophys. Res. Commun.* **369**, 195-207.

George, C. H. and Lai, F. A. (2007). Developing new anti-arrhythmics: clues from the molecular basis of cardiac ryanodine receptor (RyR2) Ca2+-release channel dysfunction. *Curr. Pharm. Des.* **13**, 3195-3211.

George, C. H., Jundi, H., Thomas, N. L., Scoote, M., Walters, N., Williams, A. J. and Lai, F. A. (2004). Ryanodine receptor regulation by intramolecular interaction between cytoplasmic and transmembrane domains. *Mol. Biol. Cell* **15**, 2627-2638.

Ikemoto, N. and Yamamoto, T. (2002). Regulation of calcium release by interdomain interaction within ryanodine receptors. *Front. Biosci.* **7**, d671-d683.

Jeyakumar, L. H., Ballester, L., Cheng, D. S., McIntyre, J. O., Chang, P., Olivey, H. E., Rollins-Smith, L., Barnett, J. V., Murray, K., Xin, H.-B. et al. (2001). FKBP binding characteristics of cardiac microsomes from diverse vertebrates. *Biochem. Biophys. Res. Commun.* **281**, 979-986.

Kobayashi, S., Yano, M., Suetomi, T., Ono, M., Tateishi, H., Mochizuki, M., Xu, X., Uchinoumi, H., Okuda, S., Yamamoto, T. et al. (2009). Dantrolene, a therapeutic agent for malignant hyperthermia, markedly improves the function of failing cardiomyocytes by stabilizing interdomain interactions within the ryanodine receptor. *J. Am. Coll. Cardiol.* **53**, 1993-2005.

Kobayashi, S., Yano, M., Uchinoumi, H., Suetomi, T., Susa, T., Ono, M., Xu, X., Tateishi, H., Oda, T., Okuda, S. et al. (2010). Dantrolene, a therapeutic agent for malignant hyperthermia, inhibits catecholaminergic polymorphic ventricular tachycardia in a RyR2(R2474S/+) knock-in mouse model. *Circ. J.* **74**, 2579-2584.

Lai, F. A., Misra, M., Xu, L., Smith, H. A. and Meissner, G. (1989). The ryanodine receptor-Ca^{2+} release channel complex of skeletal muscle sarcoplasmic reticulum. Evidence for a cooperatively coupled, negatively charged homotetramer. *J. Biol. Chem.* **264**, 16776-16785.

Liu, Z., Zhang, J., Sharma, M. R., Li, P., Chen, S. R. and Wagenknecht, T. (2001). Three-dimensional reconstruction of the recombinant type 3 ryanodine receptor and localization of its amino terminus. *Proc. Natl. Acad. Sci. USA* **98**, 6104-6109.

Mackrill, J. J., Challiss, R. A., O'connell, D. A., Lai, F. A. and Nahorski, S. R. (1997). Differential expression and regulation of ryanodine receptor and myo-inositol 1,4,5-trisphosphate receptor Ca^{2+} release channels in mammalian tissues and cell lines. *Biochem. J.* **327**, 251-258.

Masumiya, H., Wang, R., Zhang, J., Xiao, B. and Chen, S. R. (2003). Localization of the 12.6-kDa FK506-binding protein (FKBP12.6) binding site to the NH2-terminal domain of the cardiac Ca^{2+} release channel (ryanodine receptor). *J. Biol. Chem.* **278**, 3786-3792.

Paul-Pletzer, K., Yamamoto, T., Bhat, M. B., Ma, J., Ikemoto, N., Jimenez, L. S., Morimoto, H., Williams, P. G. and Parness, J. (2002). Identification of a dantrolene-binding sequence on the skeletal muscle ryanodine receptor. *J. Biol. Chem.* **277**, 34918-34923.

Paul-Pletzer, K., Yamamoto, T., Ikemoto, N., Jimenez, L. S., Morimoto, H., Williams, P. G., Ma, J. and Parness, J. (2005). Probing a putative dantrolene-binding site on the cardiac ryanodine receptor. *Biochem. J.* **387**, 905-909.

Serysheva, I. I., Ludtke, S. J., Baker, M. L., Cong, Y., Topf, M., Eramian, D., Sali, A., Hamilton, S. L. and Chiu, W. (2008). Subnanometer-resolution electron cryomicroscopy-based domain models for the cytoplasmic region of skeletal muscle RyR channel. *Proc. Natl. Acad. Sci. USA* **105**, 9610-9615.

Stewart, R., Zissimopoulos, S. and Lai, F. A. (2003). Oligomerization of the cardiac ryanodine receptor C-terminal tail. *Biochem. J.* **376**, 795-799.

Tang, Y., Tian, X., Wang, R., Fill, M. and Chen, S. R. (2012). Abnormal termination of Ca2+ release is a common defect of RyR2 mutations associated with cardiomyopathies. *Circ. Res.* **110**, 968-977.

Thireau, J., Pasquié, J.-L., Martel, E., Le Guennec, J.-Y. and Richard, S. (2011). New drugs vs. old concepts: a fresh look at antiarrhythmics. *Pharmacol. Ther.* **132**, 125-145.

Tung, C. C., Lobo, P. A., Kimlicka, L. and Van Petegem, F. (2010). The amino-terminal disease hotspot of ryanodine receptors forms a cytoplasmic vestibule. *Nature* **468**, 585-588.

Uchinoumi, H., Yano, M., Suetomi, T., Ono, M., Xu, X., Tateishi, H., Oda, T., Okuda, S., Doi, M., Kobayashi, S. et al. (2010). Catecholaminergic polymorphic ventricular tachycardia is caused by mutation-linked defective conformational regulation of the ryanodine receptor. *Circ. Res.* **106**, 1413-1424.

Wang, J. P., Needleman, D. H., Seryshev, A. B., Aghdasi, B., Slavik, K. J., Liu, S.-Q., Pedersen, S. E. and Hamilton, S. L. (1996). Interaction between ryanodine and neomycin binding sites on Ca^{2+} release channel from skeletal muscle sarcoplasmic reticulum. *J. Biol. Chem.* **271**, 8387-8393.

Wang, R., Chen, W., Cai, S., Zhang, J., Bolstad, J., Wagenknecht, T., Liu, Z. and Chen, S. R. W. (2007). Localization of an $NH_{(2)}$-terminal disease-causing mutation hot spot to the "clamp" region in the three-dimensional structure of the cardiac ryanodine receptor. *J. Biol. Chem.* **282**, 17785-17793.

Wu, Y., Aghdasi, B., Dou, S. J., Zhang, J. Z., Liu, S. Q. and Hamilton, S. L. (1997). Functional interactions between cytoplasmic domains of the skeletal muscle Ca^{2+} release channel. *J. Biol. Chem.* **272**, 25051-25061.

Yano, M., Yamamoto, T., Kobayashi, S. and Matsuzaki, M. (2009). Role of ryanodine receptor as a Ca^{2}(+) regulatory center in normal and failing hearts. *J. Cardiol.* **53**, 1-7.

Yin, C. C. and Lai, F. A. (2000). Intrinsic lattice formation by the ryanodine receptor calcium-release channel. *Nat. Cell Biol.* **2**, 669-671.

Yin, C. C., Blayney, L. M. and Lai, F. A. (2005). Physical coupling between ryanodine receptor-calcium release channels. *J. Mol. Biol.* **349**, 538-546.

Zissimopoulos, S. and Lai, F. A. (2005). Interaction of FKBP12.6 with the cardiac ryanodine receptor C-terminal domain. *J. Biol. Chem.* **280**, 5475-5485.

Zissimopoulos, S. and Lai, F. (2007). Ryanodine receptor structure, function and pathophysiology. In *Calcium: A Matter of Life or Death*, Vol. 41, pp. 287-342. Oxford: Elsevier.

Zissimopoulos, S., White, J., Cheung, I., Stewart, R. and Lai, F. A. (2005). Oligomerisation of the cardiac ryanodine receptor amino-terminus. *Biophys. J.* **88**, 270A.

Zissimopoulos, S., West, D. J., Williams, A. J. and Lai, F. A. (2006). Ryanodine receptor interaction with the SNARE-associated protein snapin. *J. Cell Sci.* **119**, 2386-2397.

Zissimopoulos, S., Docrat, N. and Lai, F. A. (2007). Redox sensitivity of the ryanodine receptor interaction with FK506-binding protein. *J. Biol. Chem.* **282**, 6976-6983.